

JET PRODUCTION STUDIES AT COLLIDERS

ROBERT HIROSKY

University of Virginia

Charlottesville, VA

E-mail: Hirosky@Virginia.Edu

An overview of jet production, measurement techniques, and recent physics results from colliders is presented. Analyses utilizing jets and boson plus jets final states are included and implications of the data are discussed. The results presented here are a snapshot of those available at the time of the PIC 2012 conference in September 2012.

1 Introduction

Hadronic jets are a key signature of strong interactions between constituent partons in high energy hadron collisions. The framework of perturbative quantum chromodynamics (pQCD) describes the partonic cross sections [1] for hard scattering at large momentum transfers and we have witnessed substantial progress in both experimental and theoretical understanding of such processes throughout the past two decades. The production amplitudes for various final states depend on the convolution of parton level cross sections with experimentally-determined parton distribution functions (PDFs) [2]. Pictorially jet production in hadron collisions can be modeled as in Fig. 1. Matrix elements (MEs) for the hard interaction are available to (next-to-)next-to-leading-order, (N)NLO, (next-to-)next-to-leading-logarithm, (N)NLL, for many processes and phenomenological models tuned to data can be used to account for hadronization effects.

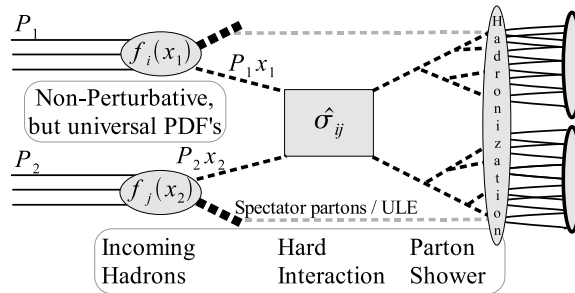


Figure 1. Jet production in hadron collisions. Matrix elements for the hard scatter are available at (N)NLO/(N)NLL for many processes under study. Non-perturbative parton distribution functions and final state hadronization are factorized from the hard scattering cross section in calculating production rates at colliders.

Jet production processes include a wide range of phenomena. In addition to purely partonic final states, a mix of strong, weak, and electromagnetic vertices may be present. These final states are used to study diverse topics such as, the performance of pQCD, strong dynamics and couplings, hadron structure and compositeness scales, hadronic decay modes of short-lived particles, signatures for new massive states, etc. Furthermore, the precise knowledge of standard model production rates and kinematic properties in jet final states is a prerequisite for achieving highest sensitivity in many searches for new physics and rare standard model (SM) processes. This paper reviews the status of recent QCD studies from collider experiments at the LHC and Tevatron. Discussions of jets in deep inelastic scattering, photoproduction, and e^+e^- collisions are included in the contributions by M. Wang and R. Kogler to these proceedings. An overview of the status of modern PDF models is presented in the contribution by Johannes Blümlein.

2 Jet Identification

Although hadronic jets arise from the hadronization of elementary quarks and gluons and are highly correlated with the four-vectors of their parent particle, it is important to note that, unlike elementary particles, jets are ultimately defined by the algorithm used in their reconstruction. Therefore, different algorithms will in general identify a different set of jets in the same data. A good jet algorithm will satisfy the following properties: (1) deliver consistent results when applied to partons, particles from hadronization, or to detector-level information such as tracks or energy clusters; (2) be relatively stable with respect to detector noise and additional energy deposits from hadron remnants, coincidental soft collisions, and soft parton radiation; (3) have good energy and angular resolution and be relatively straightforward to calibrate. Typical approaches to jet reconstruction employ cone-based or recombinant algorithms. An extensive review of modern jet algorithms can be found in Ref. [3] and references therein.

In cone-based algorithms fixed cones with vertices set to the primary interaction point are used to select objects to form the jet. Typically the angular position of the cone is iterated until its geometric center (in azimuthal angle ϕ and rapidity y) matches the location of the combined four-vector or weighted average position of the enclosed objects (energy deposits, tracks, particle four-vectors, etc). The cone algorithms primarily used at the Tevatron are described in Refs. [4] and [5] for the D0 and CDF Experiments, respectively.

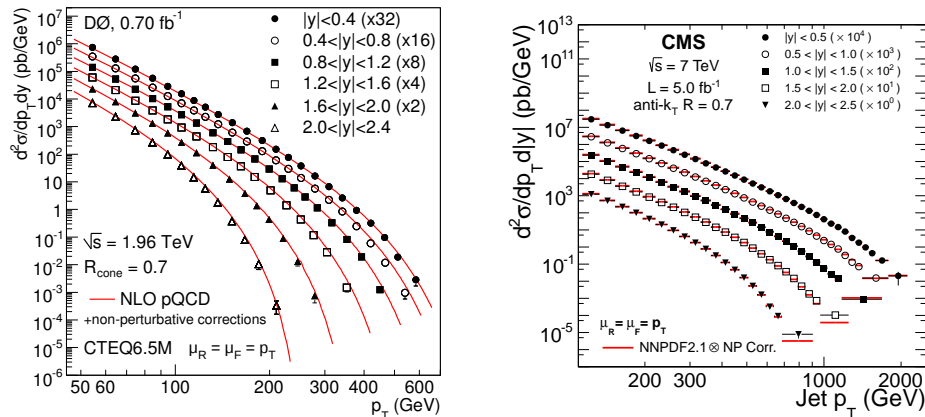
Recombination or sequential clustering algorithms successively merge objects based on spatial and/or relative transverse momenta criteria. Clusters are then successively merged until satisfying some well defined stopping criteria and the jet four-vector is calculated by summing all combined objects. Examples are the k_T [6] algorithms and also the anti- k_T algorithm [7] which is frequently employed in analyses from the LHC.

While various experiments and individual analyses can employ different algorithms or choices of parameters to control their performance, each measurement is necessarily compared to theory or Monte Carlo (MC) using consistent algorithm definitions.

3 Inclusive Jets and Dijet Production

Measures of inclusive jet production are sensitive to a combination of QCD matrix elements describing the hard parton scattering and initial state parton distribution functions (PDFs). Inclusive measures allow tests of perturbative QCD over wide ranges of parton momentum exchange (Q) and their sensitivity to wide ranges of parton momentum fractions (x) can provide further constraints to PDF models. Furthermore, because the strong coupling (α_s) depends on the momentum exchange scale, these measurements provide information about the running of the coupling to our largest accessible momentum scales.

Measurements of the inclusive jet cross section plotted differentially in bins of jet transverse momentum (p_T) and rapidity (y) are shown in Figs. 2(a) and 2(b) for the D0 [8] and CMS [9] Experiments, respectively. These results illustrate the remarkable success of perturbative QCD and phenomenological understanding of proton structure in high energy collisions, spanning 8–9 orders in jet p_T . In each case experimental results are compared to theory calculated to next-to-leading-order in QCD.



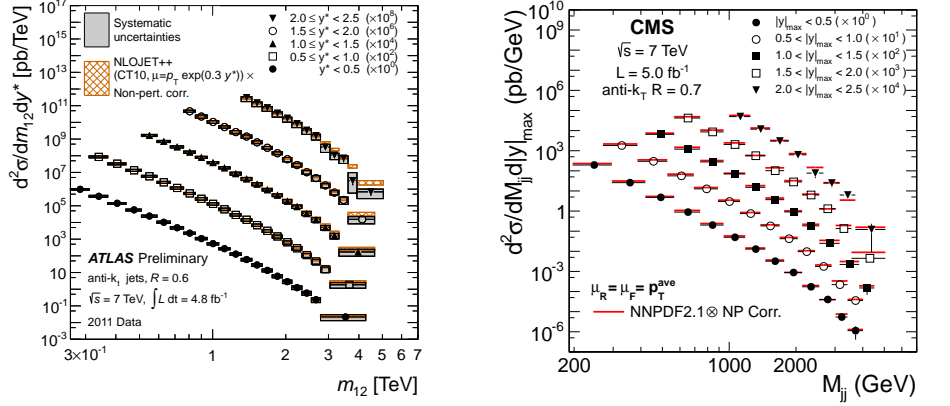
(a) Inclusive jet cross section measurements by the D0 Experiment as a function of jet p_T in six $|y|$ bins.

(b) Inclusive jet cross section measurements by the CMS Experiment as a function of jet p_T in five $|y|$ bins.

Figure 2. Measures of the inclusive jet cross section at the Tevatron and LHC.

Measurements of the dijet mass spectra in LHC collisions at 7 TeV presented by the ATLAS [10] and CMS [9] Experiments are shown in Fig. 3. Preliminary results at 8 TeV are in agreement with these [11]. Again, detailed comparisons to predictions from pQCD show good agreement between data and theory.

Examples of the relative precision of the inclusive jet measurements are shown in Figs. 4(a) and 4(b). In these results, illustrating D0 and CMS measurements, the experimental uncertainties are similar to or significantly smaller than those associated with PDF models, showing that the data can provide significant con-

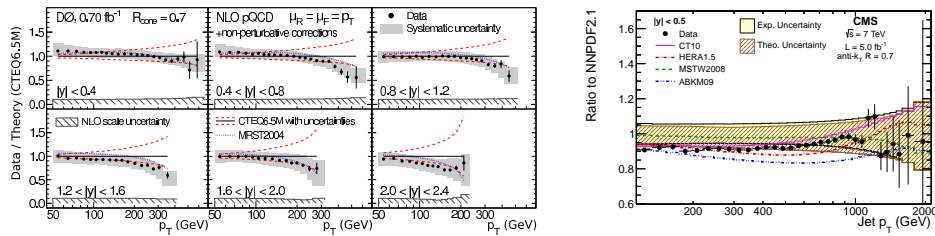


(a) ATLAS measurement of dijet double-differential cross section plotted versus invariant mass of the leading p_T jets. Measurements are binned in terms of the average rapidity separation between the jets $y^* = |y_1 - y_2|/2$.

(b) CMS measurement of the dijet double-differential cross section plotted versus invariant mass of the leading p_T jets. Measurements are binned in terms of the maximum rapidity of the two jets $|y_{\text{max}}| = \max(|y_1|, |y_2|)$.

Figure 3. Measurements of the dijet mass cross sections at the LHC.

straints on the PDFs. A similar comparison from the ATLAS Experiment is shown in Fig 6(a), but considering the dijet mass spectrum. This also illustrates the interest of pushing experimental measurements to more extreme regions of phase space for jet production. For dijet pairs at the maximum measured rapidity separation, the agreement of theory and experiment is clearly observed to break down at large invariant mass, which may indicate the need for higher order terms to accurately describe the data.



(a) D0 data divided by theory for the inclusive jet cross section as a function of jet p_T in six $|y|$ bins.

(b) CMS ratio of inclusive jet cross section ($|y| < 0.5$) to the theory prediction with NNPFD2.1 [12] PDFs.

Figure 4. Examples of relative precision of experimental measures and theory calculations on inclusive jet cross sections.

4 Measurements in Multijet Final States

Measurements using multijet final states are powerful tools to test the applicability of pQCD calculations and to examine the running of the strong coupling constant. The D0 Experiment reported an analysis of multijet final states using a new observable [13], $R_{\Delta R}$, which is computed as a ratio of cross sections as illustrated in Fig. 5. This observable measures the number of neighboring jets that accompany a jet of given p_T within an angular region ΔR defined in (y, ϕ) space. Because PDF dependencies largely cancel in the ratio, these results can be used to extract a measure of α_s , almost independent of initial assumptions on the renormalization group equation (RGE). The measured results are displayed in Fig. 7(a) in bins of ΔR , the search region for neighboring jets, and p_{Tmin}^{nbr} , the minimum p_T for inclusion of neighboring jets as a function of inclusive jet p_T . In each ΔR interval the value of $R_{\Delta R}$ increases with jet p_T until approaching the kinematic limit.

Event shape studies [14] by the CMS Experiment include a measure of the central transverse thrust, $\tau_{\perp, C}$ which probes QCD radiative processes and is mostly sensitive to the modeling of two- and three-jet topologies. The central transverse thrust defined in Refs. [14,15] is a measure of radiation along an event's transverse thrust axis. The CMS measurement is shown in Fig. 6(b) compared to predictions from five MC simulations. The parton shower (PS) MC generators PYTHIA [16] and HERWIG [17] show generally good agreement with the data, except for PYTHIA version 8 which shows some discrepancy at extreme values of $\tau_{\perp, C}$. The disagreement in calculations by ALPGEN [18] and MADGRAPH [19] implies that the regime of high jet p_T and multiplicity where the explicit higher final state parton multiplicity ME calculations of these generators significantly improves upon a pure PS approach has not been reached in these data.

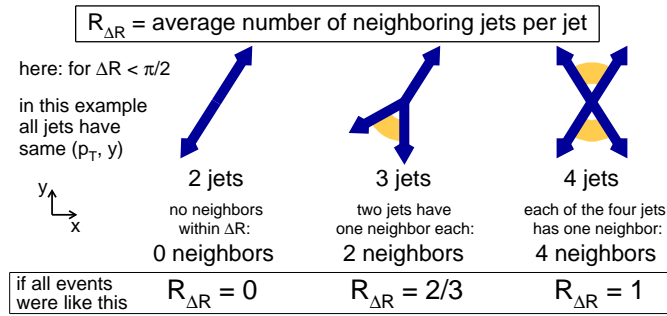
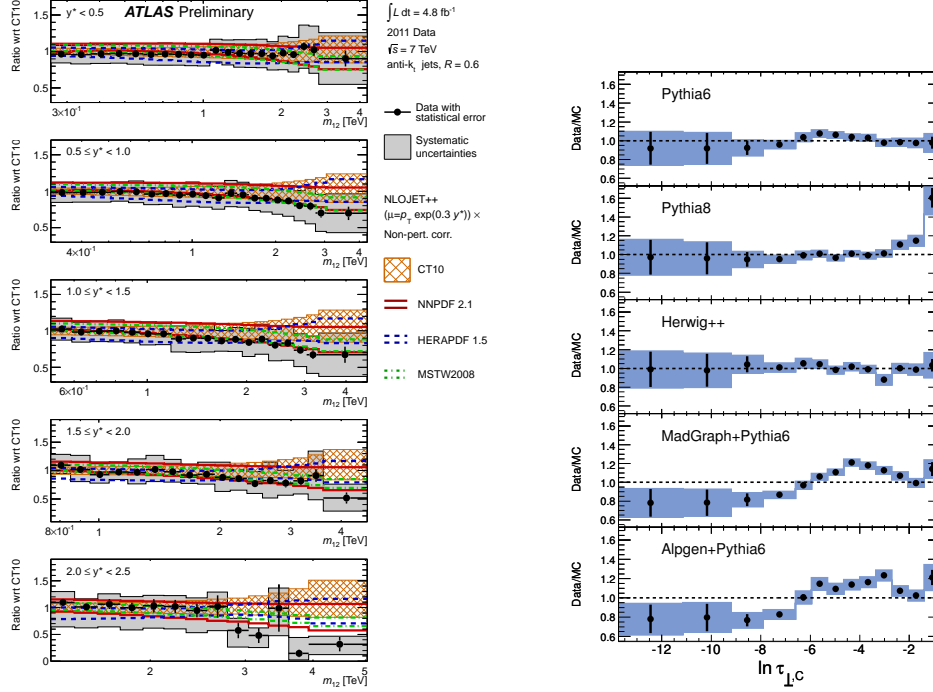


Figure 5. Illustration of the variable $R_{\Delta R}(p_T, \Delta R, p_{Tmin}^{nbr}) = \frac{\sum_{i=1}^{N_{jet}(p_T)} N_{nbr}^{(i)}(\Delta R, p_{Tmin}^{nbr})}{N_{jet}(p_T)}$, which measures the number of neighboring jets accompanying a jet satisfying a given requirement on transverse momentum.



(a) ATLAS ratios of dijet double-differential cross section, shown as a function of dijet invariant mass, to the theoretical prediction obtained using NLOJET++ [20] with the CT10 [21] PDF set.

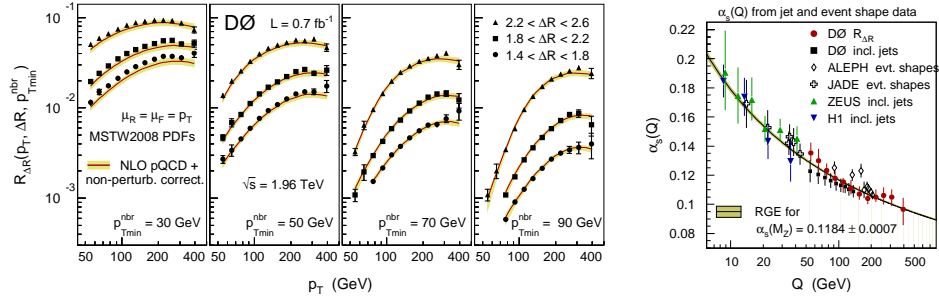
(b) CMS Distributions of the logarithm of the central transverse thrust for events with leading jet between 125 and 250 GeV. Results in data are compared to predictions from five MC simulations. Shaded bands represent the quadratic sum of the statistical and systematic uncertainties.

Figure 6. Measures of dijet and multijet distributions at the LHC.

5 Measure of the Running of the Strong Coupling Constant

Precise measures of jet production can be used to test the running of the strong coupling constant α_s , reaching significantly higher scales than are accessible by other methods. While the running of α_s is predicted by the RGE, it remains the least precisely known of the fundamental couplings. Furthermore, its running can be modified at large Q by the presence of new physics, such as the presence of extra spatial dimensions.

Because jet cross sections depend on a combination the strong coupling and parton distributions, the extraction of α_s requires theory predictions as a continuous function of α_s used in both the matrix elements and PDFs. The dependence of the PDFs on α_s is parameterized by interpolating theory results based on PDF sets determined using incremental steps in α_s . Correlated systematic experimental and theoretical uncertainties are treated via the Hessian approach [22] and α_s values are determined by minimizing a χ^2 function with respect to α_s and nuisance parameters



(a) Measurement of $R_{\Delta R}$ for different intervals in the ΔR search region for neighboring jets and requirements on p_{Tmin}^{nbr} . (b) Measurements of the strong coupling constant α_s as a function of momentum transfer Q .

Figure 7. D0 measurements of (a) multijet distributions and (b) extraction of α_s , determined from D0 inclusive jets and event shapes.

for the uncertainties. Results are shown in Fig. 7(b) for this measurement and an earlier determination [23] using the D0 inclusive jet cross section. Additional determinations of the strong coupling constant using inclusive and multijet cross sections in deep inelastic scattering data are presented in the contribution by R. Kogler to these proceedings.

6 Jets in Association with Vector Bosons

A great deal of progress has been made in measurements of jets in association with vector bosons (V) in recent years. These processes provide valuable tests of fixed order and ME+PS predictions and their precise measurements provide important constraints on backgrounds for rare SM physics and searches for evidence of new physics processes. The production of $V+n$ -jet final states provides a handle to study multiscale QCD processes and plays a significant role as background in searches for beyond the standard model phenomena and many Higgs boson measurement channels. Theoretical uncertainties on their production rates and kinematics introduce large uncertainties and limit our ability to identify new physics processes.

A large variety of Monte Carlo programs are compared to data to test the applicability of perturbative calculations and phenomenologically tuned models in diverse regions of phase space for $V+n$ -jet final states. Examples of MC calculations compared to these data include: LO parton shower MC such as PYTHIA, leading-order matrix element plus parton shower matched MC such as ALPGEN and SHERPA [24], calculations employing all-order resummation of wide angle emissions (HEJ [25]), and next-to-leading order pQCD predictions for the production of a vector boson plus multiple parton final states: BLACKHAT+SHERPA [26] and ROCKET+MCFM [27,28].

Figure 8 shows examples of measurements performed at the D0 [29] and ATLAS [30] Experiments. The D0 measurement of the W boson transverse momentum for inclusive jet multiplicity bins is shown in Fig. 8(a). Predictions from BLACKHAT-

SHERPA and HEJ show good agreement for all jet multiplicities. At jet p_T below the threshold of 20 GeV, nonperturbative effects dominate and the fixed order calculations are expected to be unreliable.

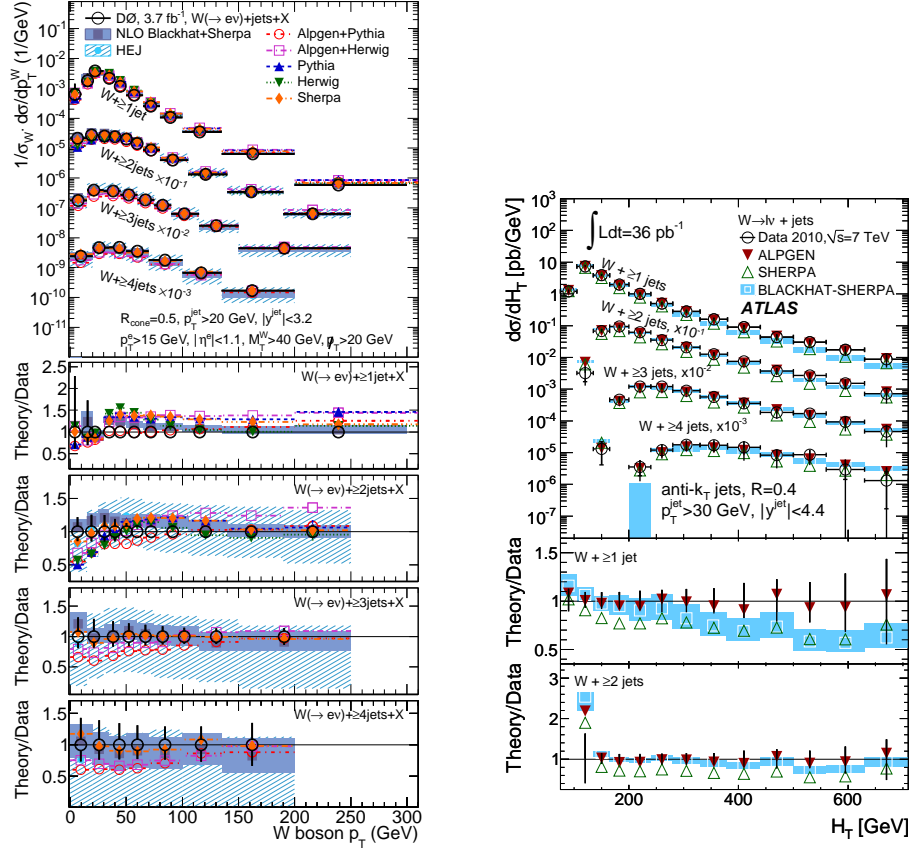
The measured H_T distribution (scalar p_T sum of reconstructed physics objects) for W events with one or more jets, measured at ATLAS, is shown in Fig. 8(b). The prediction, calculated inclusively at NLO by BLACKHAT-SHERPA, does not describe the data, due to the limited order of the matrix element calculation, which does not include three or more real emissions of final-state partons. The LO ME calculation of ALPGEN with up to five final-state partons, describes the data well. A study described in Ref. [30] considers improvements with a modified treatment of BLACKHAT-SHERPA predictions introducing higher-order NLO terms describing higher real emission multiplicities. A matching scheme is developed and required to reduce double-counting of cross sections, illustrating the challenges of comparing NLO calculations to complex inclusive jet variables like H_T .

The D0 Experiment reported a first measurement of the probability of emission of a third jet in inclusive $W + 2$ -jet events as a function of the dijet rapidity separation of the two leading jets. This measurement, shown in Fig. 9(a), is presented in both p_T - and rapidity-ordered scenarios, and a hybrid result considering the probability of additional jet emission in the rapidity interval defined by the two leading p_T jets. Resummation predictions from HEJ are best able to describe both the rate and shape across the full rapidity range.

Studies involving differential properties in Z +jet production are similarly of interest to those involving W +jets. Using leptonic decay modes of the Z boson allows for selection of low background samples and provides precise constraints on the scale of hadronic recoil in the event. CDF reported measured Z +jet cross sections compared to NLO QCD combined with NLO EW calculations [31]. A measurement of the Z +jet cross section versus p_T of the leading lepton from the Z decay [32] is shown to be well modeled in Fig. 9(b).

Measurements of W/Z plus heavy flavor jets were also presented by experiments at the Tevatron and LHC. These processes are important backgrounds to measurement of associated Higgs boson production and suffer from significant theoretical uncertainty on their production. An earlier measurement [33] of $W + b$ -jet production using 1.9 fb^{-1} of Tevatron Run 2 data by the CDF Experiment is shown in Fig. 10(a), where the exclusive $W + b$ -jet cross section is determined after removal of c -jet and light-flavor jet background using templates based on the secondary vertex mass in b -tagged jets. This result yielded a cross section of about three standard deviations in excess of SM predictions at NLO accuracy for events with exactly one or two jets with $E_T > 20 \text{ GeV}$ and lepton from W decay with similar requirement. A more recent measurement [34] performed by ATLAS considers exclusive production of $W + b$ -jet events for one, two, and one or two identified b jets. The results shown in Fig. 10(b) are in good agreement with NLO predictions for the one jet exclusive case, and agree to within 1.5 s.d. for the other categories. A measurement [35] provided by the D0 Experiment following the conference finds the inclusive $W + b$ -jet production cross section to be in agreement with NLO predictions within scale and PDF uncertainties.

The CMS Experiment provided a recent study [36] of the $Z/\gamma^* + b$ -jet cross



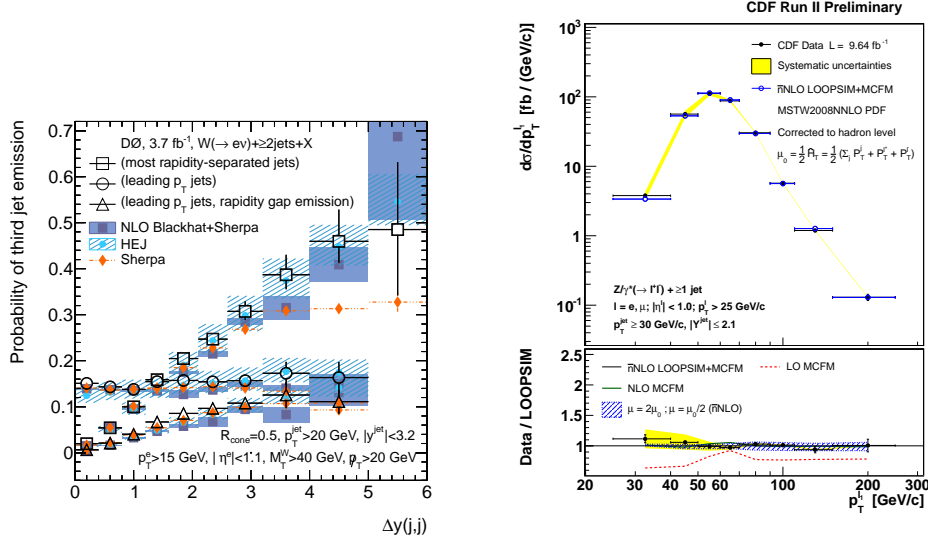
(a) D0 measurement of the W boson transverse momentum distributions in inclusive $W + n$ -jet events for $n = 1 - 4$ compared to various theoretical predictions.

(b) ATLAS W +jets cross section as a function of H_T for separate jet multiplicities. Results are compared to predictions from ALPGEN, SHERPA, and BLACKHAT-SHERPA.

Figure 8. $W + n$ -jet measurements from the D0 and ATLAS Experiments.

sections using 2.1 fb^{-1} of pp collisions at $\sqrt{s} = 7 \text{ TeV}$ and additional results were provided by the CDF Experiment [37] using the full CDF data set. Figure 11(a) shows the p_T of the bb system in an event sample selected to identify $Z + bb$ final states at CMS. In general the CMS results indicate that predictions based on the MADGRAPH event generator interfaced with PYTHIA and normalized to the NNLO inclusive cross section provide a fair description of the data.

Finally a measurement [38] of the differential cross section for photon+ b -jet production was provided by the D0 Experiment. The results are summarized in Fig. 11(b) which shows the ratios of data to the NLO QCD calculations and different MC simulations to the same NLO calculations. The observed variance with respect to several PDF models is also shown. The data can only be described by



(a) D0 measurement of the probability of emission of a third jet in inclusive $W + 2$ -jet events for various definitions of rapidity interval as described in the text.

(b) CDF measured cross section in $Z/\gamma^* + \geq 1$ jet events as a function of leading lepton p_T .

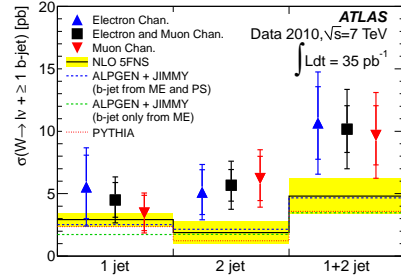
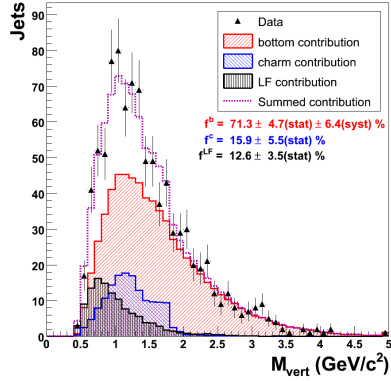
Figure 9. Measurements of W and Z +jets differential cross sections from the Tevatron.

including higher order corrections into the NLO QCD predictions, such as those currently present as additional real emissions in the SHERPA MC generator. This is an interesting measurement to compare with future results from the LHC, since the production of photon plus heavy flavor events at the Tevatron is dominated by final state gluon splitting $q\bar{q} \rightarrow \gamma g (g \rightarrow b\bar{b})$, while at the LHC $bq \rightarrow b\gamma$ dominates for most of the experimentally accessible p_T ranges.

7 Soft QCD

Another area of study at the LHC and Tevatron experiments involves nonperturbative processes. Reviews of measurements involving multiparton interactions and total cross sections are presented respectively by E. Dobson and N. Cartiglia in these proceedings. Presented here is a recent measurement [39] by the CMS experiment of the contribution from diffractive dijet production to the inclusive dijet cross section. Events are selected to contain at least two jets with $p_T > 20$ GeV with the leading jet satisfying $|\eta^{\text{jet}}| < 4.4$ [40]. The quantity^a $\xi = M_X^2/s$, which approximates the fractional momentum loss of the scattered proton in single diffractive events is approximated ($\tilde{\xi}$) from the energies and longitudinal momenta of all

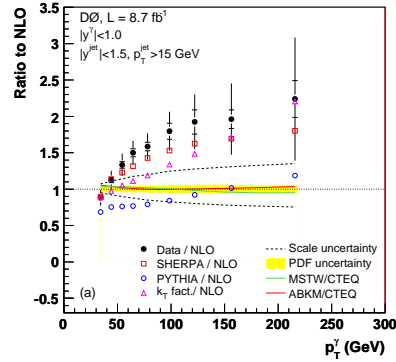
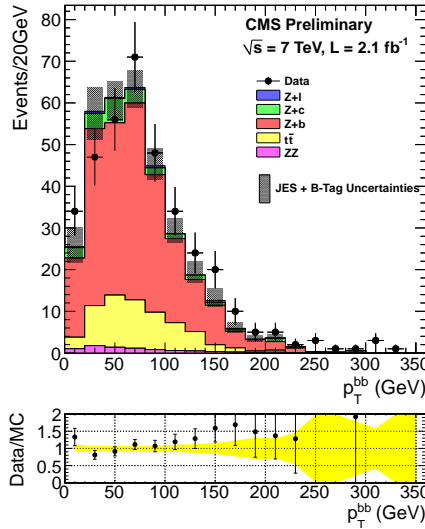
^aIn this study of diffractively produced events M_X represents the mass of the jet system which is separated from the an opposing scattered proton by a large rapidity gap



(a) CDF fit to selected events in $W+b$ -jet analysis, based on a maximum likelihood of the ratio of vertex mass distributions for signal and background in b tagged jets in the selected data sample in 1.9 fb^{-1} of Tevatron Run 2 data.

(b) ATLAS measurement of the $W+b$ -jet cross section in the 1, 2, and 1+2 jet exclusive bins. The measurements are compared with NLO predictions in pQCD.

Figure 10. CDF and ATLAS measurements of the $W+b$ production cross section.

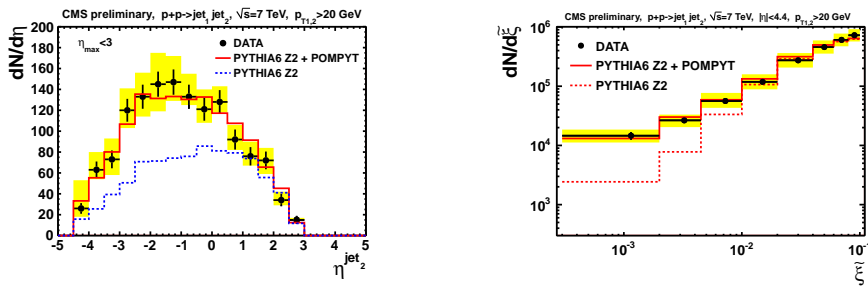


(a) CMS measurement of the p_T of the b -jet system in events selected to identify $Z+bb$ final states.

(b) D0 ratio of $\gamma+b$ differential cross section between data and NLO QCD predictions with uncertainties for the rapidity region $|y^\gamma| < 1.0$.

Figure 11. Measures of the $Z+b$ and $\gamma+b$ cross sections from CMS and D0.

particle flow [41] objects measured in the region $|\eta| < 4.9$. Figure 12(a) shows the η distribution for the second leading jet after application of a requirement to enhance the diffractive contribution to the measured cross section. This requirement [39] is equivalent to imposing a pseudorapidity gap of at least 1.9 units, enhancing the diffractive component in the data, and selecting events with the jets mainly in the hemisphere opposite to that of the gap. A combination of PYTHIA6 with tune Z2 and single diffractive events modeled with POMPYT [42] is found to agree with the data reasonably well. Figure 12(b) shows the reconstructed ξ distribution compared to detector-level MC predictions with and without the inclusion of diffractive dijet production.



(a) CMS reconstructed pseudorapidity distributions of the second-leading jets, after imposing a pseudorapidity gap requirement, and compared to detector-level MC predictions with and without diffractive dijet production.

(b) CMS reconstructed ξ distribution compared to detector-level MC predictions with and without diffractive dijet production.

Figure 12. CMS study of diffractive dijet production.

8 Conclusions

Remarkable progress continues in measurements concerned with jet production. Unprecedented data sets, measurement precision, and improvements in theory have enabled ever more rigorous tests of standard model predictions and the extraction of fundamental parameters such as the strong coupling constant at ever increasing momentum scales. These data inform models for PDFs and constrain important backgrounds for rare SM and new physics searches. They further test the applicability of fixed order perturbative calculations, parton shower MC, and other models over an exceptionally large phase space of final states. As shown in this brief sampling of results, numerous areas require work understand the effects of higher order and nonperturbative processes to improve our modeling of the data and further enhance sensitivities to new physics processes.

I wish to thank the organizers of Physics in Collision 2012 for giving me the opportunity to present these results and the ATLAS, CDF, CMS, D0, HERA, and ZEUS collaborations for providing the results included in this talk.

References

1. F. Aversa *et al.*, Phys. Rev. Lett **65**, 401 (1990);
W. T. Giele, E.W. N. Glover, and D. A. Kosower, Phys. Rev. Lett **73**, 2019 (1994);
D. Ellis, Z. Kunszt, and D. E. Soper, Phys. Rev. Lett **64**, 2121 (1990).
2. See contribution from J. Blümlein in these proceedings.
3. M. Cacciari, G. P. Salam, G. Soyez, CERN-PH-TH/2011-297, arXiv:1111.6097.
4. V. M. Abazov *et al.* (D0 Collaboration), Phys. Rev. D **85** (2012) 052006.
5. A. Abulenci *et al.* (CDF Collaboration), Phys. Rev. D **74**, 071103 (2006).
6. S. Catani, Y. L. Dokshitzer, M. H. Seymour and B. R. Webber, Nucl. Phys. B **406**, 187 (1993);
S. D. Ellis and D. E. Soper, Phys. Rev. D **48**, 3160 (1993).
7. M. Cacciari and G. P. Salam, JHEP **0804** 005 (2008).
8. V. Abazov *et al.* (D0 Collaboration), Phys. Rev. D **85**, 052006 (2012); V. Abazov *et al.* (D0 Collaboration), Phys. Rev. Lett. **101**, 062001 (2008).
9. S. Chatrchyan *et al.* (CMS Collaboration), [arXiv:1212.6660].
10. G. Aad *et al.* (ATLAS Collaboration), Phys. Rev. D **86** (2012) 014022.
11. B. Chapleau, presentation at 36th International Conference for High Energy Physics, July 2012,
<http://indico.cern.ch/conferenceDisplay.py?confId=181298>.
12. R. D. Ball *et al.*, Nucl.Phys. B **838**, 136 (2010).
13. V. Abazov *et al.* (D0 Collaboration), Phys. Lett. B **718**, 56 (2012).
14. V. Khachatryan *et al.* (D0 Collaboration), Phys. Lett. B **699** 48-67 (2011).
15. A. Banfi, G.P. Salam, G. Zanderighi, JHEP 1006 (2010) 038.
16. T. Sjostrand, S. Mrenna and P. Z. Skands, J. High Energy Phys. 05, 26 (2006).
17. G. Marchesini *et al.*, *The Herwig Event Generator*, Comp. Phys. Comm. **67** (1992) 465.
18. M. L. Mangano *et al.*, J. High Energy Phys. 07, 1 (2003).
19. J. Alwall, M. Herquet, F. Maltoni, O. Mattelaer, T. Stelzer, J. High Energy Phys. **06** (2011) 1029.
20. Z. Nagy, Phys. Rev. Lett. **88** (2002) 122003 [hep-ph/0110315]; Phys. Rev. D **68** (2003) 094002.
21. J. Gao *et al.*, arXiv:1302.6246.
22. A. Cooper-Sarkar and C. Gwenlan, in Proceedings of the Workshop: HERA and the LHC, Part A, edited by A. De Roeck and H. Jung, Geneva, Switzerland (2005), CERN- 2005-014, DESY-PROC-2005-01, arXiv:hep-ph/0601012, see part 2, section 3.
23. V. Abazov *et al.* (D0 Collaboration), Phys. Rev. D **80**, 111107 (2009).
24. T. Gleisberg *et al.*, J. High Energy Phys. 02, 7 (2009).
25. J. R. Andersen and J. M. Smillie, J. High Energy Phys. 01, 39 (2010); J. R. Andersen and J. M. Smillie, Phys. Rev. D **81**, 114021 (2010); J. R. Andersen and J. M. Smillie, Nucl. Phys. Proc. Suppl. **205**, 205 (2010); J. R. Andersen and J. M. Smillie, J. High Energy Phys. 06, 10 (2011); J. R. Andersen, T. Hapola and J. M. Smillie, J. High Energy Phys. 09, 047 (2012).

26. C. F. Berger, et al., Phys. Rev. Lett. 102, 222001 (2009); C. F. Berger et al., Multi-jet cross sections at NLO with BlackHat and Sherpa, arXiv:0905.2735 [hep-ph]; C. F. Berger et al., Phys. Rev. D 80, 074036 (2009).
27. J. M. Campbell and R. K. Ellis, Phys. Rev. D 65, 113007 (2002); J. M. Campbell, R. K. Ellis and D. L. Rainwater, Phys. Rev. D 68, 94021 (2003).
28. R. K. Ellis et al., J. High Energy Phys. 01, 12 (2009); W. T. Giele and G. Zanderighi, J. High Energy Phys. 06, 38 (2008).
29. V. Abazov *et al.* (D0 Collaboration), [arXiv:1302.6508].
30. G. Aad *et al.* (ATLAS Collaboration), Phys. Rev. D **85** (2012) 092002.
31. A. Denner, S. Dittmaier, T. Kasprzik, A. Mück, JHEP **06** (2011) 069.
32. http://www-cdf.fnal.gov/physics/new/qcd/zjets10fb_new/NLOEW.html.
33. T. Aaltonen *et al.* (CDF Collaboration), Phys. Rev. Lett. **104** 131801 (2010).
34. G. Aad *et al.* (ATLAS Collaboration), Phys. Lett. B **707** 418 (2012).
35. V. Abazov *et al.* (D0 Collaboration), Phys. Lett. B **718** 1314 (2013).
36. S. Chatrchyan *et al.* (CMS Collaboration), J. High Energy Phys. **06** (2012) 126.
37. T. Aaltonen *et al.* (CDF Collaboration), <http://www-cdf.fnal.gov/physics/new/qcd/zbjet2012/index.html>.
38. V. Abazov *et al.* (D0 Collaboration), Phys. Lett. B **714** 32 (2012).
39. S. Chatrchyan *et al.* (CMS Collaboration), Phys. Rev. D **87** (2013) 012006.
40. The pseudorapidity is defined as $\eta = -\ln[\tan(\theta/2)]$, where θ is the polar angle with respect to one of the beam directions.
41. CMS Collaboration, CMS Physics Analysis Summary Report No. CMS-PAS-PFT-09-001, 2009.
42. P. Bruni and G. Ingelman, Diffractive hard scattering at ep and p anti-p colliders, DESY 93-187, (1993).